LA-UR-15-22317
Approved for public release; distribution is unlimited.

Title: Model Reduction and Optimization of Natural Gas Pipeline Dynamics

Author(s): Zlotnik, Anatoly V.
Backhaus, Scott N
Chertkov, Michael
Dyachenko, Sergey

Intended for: ASME Dynamic Systems and Control Conference, 2015-10-28/2015-10-30 (Columbus, Ohio, United States)

Issued: 2018-02-07 (rev.1)

**Proceedings of 2015 ASME Dynamic Systems and Control Conference**
**DSCC 2015**
**October 28–30, 2015, Columbus, OH, USA**

**DSCC2015-9683**

# MODEL REDUCTION AND OPTIMIZATION OF NATURAL GAS PIPELINE DYNAMICS

**Anatoly Zlotnik**
Center for Nonlinear Studies
Theoretical Division
Los Alamos National Laboratory
Los Alamos, NM 87545
Email: azlotnik@lanl.gov

**Sergey Dyachenko**
Department of Mathematics
The University of Arizona
Tucson, AZ 85721
Email: sdyachen@math.arizona.edu

**Scott Backhaus**
Condensed Matter & Magnet Science
Materials Physics and Applications Division
Los Alamos National Laboratory
Los Alamos, NM 87545
Email: backhaus@lanl.gov

**Michael Chertkov**
Physics of Condensed Matter & Complex Systems
Theoretical Division
Los Alamos National Laboratory
Los Alamos, NM 87545
Email: chertkov@lanl.gov

## ABSTRACT

*We derive a reduced control system model for the dynamics of compressible gas flow through a pipeline subject to distributed time-varying injections, withdrawals, and control actions of compressors. The gas dynamics PDE equations are simplified using lumped elements to a nonlinear ODE system with matrix coefficients. We verify that low-order integration of this ODE system with adaptive time-stepping is computationally consistent with solution of the PDE system using a split-step characteristic scheme on a regular space-time grid for a realistic pipeline model. Furthermore, the reduced model is tractable for use as the dynamic constraints of the optimal control problem of minimizing compression costs given transient withdrawals and gas pressure constraints. We discretize this problem as a finite nonlinear program using a pseudospectral collocation scheme, which we solve to obtain a polynomial approximation of the optimal transient compression controls. The method is applied to an example involving the Williams-Transco pipeline.*

## 1 INTRODUCTION

Recent trends compel the development of methods for modeling and optimizing transient dynamics of natural gas pipelines [1]. Advances in extraction technologies have led to abundant and inexpensive natural gas, which has resulted in rapid construction of new gas-fired electric power plants, whose gas consumption is far more variable and less predictable than that of residential and industrial consumers. This has resulted in unprecedented variability in dynamics of natural gas transmission systems, which are being subjected to transient stresses under which they were not designed to operate. A new approach to modeling such stochastic influences and reducing the risk to gas pipelines has been proposed [2]. To develop more flexible, secure, and responsive operation of gas transmission pipeline systems, it is necessary to examine them as dynamical control systems, and apply control-theoretic principles to formulate effective and tractable control techniques. Moreover, using a dynamic optimal control model that incorporates available information on time-varying gas withdrawals increases the effective capacity of a pipeline over current operating practices, and hence provides a solution to the challenge of inconsistent regional demand.

The dynamics of transient flow of natural gas in a transmission pipeline can be represented by the Euler equations for compressible gas flow in one-dimension [3, 4]. For physically relevant parameters, this system of PDEs is defined over very large scales in distance and time, and is highly nonlinear even with physical modeling simplifications [5]. As a result, transient flows in pipelines on the scale of hundreds of kilometers are problem-

atic to simulate, and many methods have been proposed [6, 7]. Indeed, pipeline simulation is an area of increasingly active research [8–10], and is of interest to gas system operators.

The ultimate goal of pipeline modeling and simulation is to optimize natural gas transmission operations by managing compressor stations and other system functions. However, the difficulty of characterizing the dynamics of transient compressible gas flow in large pipelines presents challenges for engineering, design, and operation of such systems. The effectiveness and scalability of an optimization methodology will largely depend on model reduction and discretization of the PDE constraints that represent gas dynamics over widely distributed space and time domains, and any approach is computationally intensive. Early studies of pipeline optimization [11–13] examined steady-state gas flows, in which the PDE dynamics reduce to simple algebraic relations. Recent efforts have improved and scaled up optimization techniques for similar problems [14–17]. Optimization of multi-day operations of gas pipeline networks involving transient flows was examined in several studies [18–20], and recent work has involved economic model predictive control [21, 22]. In those studies the PDE constraints are represented with implicit first order schemes in space and time, which result in very large-scale problems due to the fine discretization required to adequately resolve transients on the time-scales of interest.

In this manuscript we extend the notion of the static optimal gas flow (OGF) [16] to the transient case. The objective is to minimize the power expenditure, hence the operating cost, of compressors distributed along a gas pipeline, subject to transient injections and withdrawals along its extent, while satisfying system pressure constraints. We formulate the gas pipeline management problem of economic transient compression (ETC) as a PDE-constrained optimal control problem (OCP). The PDE constraints are then approximated by a control system derived from a model reduction for gas pipeline dynamics [23]. This modified OCP is then approximated using pseudospectral (PS) discretization [24] to yield a nonlinear program (NLP) whose decision variables are coefficients of a polynomial approximation for the control model variables. Our approach provides several advantages relative to previous methods. The representation of continuous dynamics using polynomials provides spectral accuracy, so that comparable fidelity is obtained using coarser discretization, and thus far fewer decision variables are required. In addition, the control system model can be integrated using an ODE solver to validate compression functions produced by solving the NLP.

The manuscript is organized as follows. Section 2 contains a summary of the physics of compressible gas flow in pipelines. In Section 3, we formulate the ETC OCP, and in Section 4 a reduced control system model is derived for compressible gas flow through a transmission pipeline subject to time-varying injections, withdrawals, and actions of compressors. The model is computationally validated in Section 5 through comparison to a split-step characteristic scheme on a regular space-time grid using realistic pipeline parameters. In Section 6, we reformulate the ETC OCP using the reduced model in Section 4 for the dynamic constraints. We describe implementation of the solution through approximation of the OCP by an NLP using the Legendre-Gauss-Lobatto (LGL) PS collocation method, which is summarized in Appendix A. A simple example is then used to test the method and interpret the solution. Section 7 describes a case study of a 1095 mile section of the Williams-Transco pipeline, for which the ETC solution is computed and compared to the OGF. Finally, Section 8 contains some discussion and suggests directions for future work.

## 2 GAS PIPELINE DYNAMICS

Adiabatic flow of a compressible gas in a pipeline is described by the Euler equations in one dimension [6], given by

$$\partial_t \rho + \partial_x (v\rho) = 0, \tag{1}$$

$$\partial_t (\rho v) + \partial_x (\rho v^2 + p) = -\frac{\lambda}{2D}\rho v|v| - \rho g \sin\theta, \tag{2}$$

which represent mass conservation and momentum balance. The variables are gas velocity $v$, pressure $p$, and density $\rho$, defined on a domain $x \in [0, L]$ at time $t$. The parameters are the friction factor $\lambda$, pipe diameter $D$, gravitational acceleration $g$, and pipe angle $\theta$. The terms on the right hand side of (2) aggregate friction and gravity effects. We assume that gas pressure $p$ and density $\rho$ satisfy the relation $p = \rho ZRT$, where $Z$, $R$, and $T$, are the gas compressibility factor, ideal gas constant, and temperature, respectively. Equation (2) is valid in the regime when changes in gas consumption and injections are sufficiently slow to not excite propagation of sound waves. Formally, the term $\partial_t(\rho v)$ on the left hand side is much smaller than $\partial_x(\rho v^2 + p)$. The ratio of the pressure gradient term $\partial_x p$ to the term $\partial_t(\rho v)$ is typically on the order of $1 : 0.01$ [4]. In addition, the flow velocities are much smaller than the speed of sound, $a = \sqrt{ZRT}$, so that the gas advection term $\partial_x(\rho v^2)$ can be omitted, even in comparison with the already small term $\partial_t(\rho v)$. We assume that the pipeline is level, thus ignoring the gravity term $\rho g \sin\theta$ on the right hand side of (2), and that the gas temperature is uniform along the pipeline, which yields $p = a^2\rho$. With these assumptions, (1) and (2) can be written in terms of mass flux $\phi = \rho v$ as

$$\partial_t \rho + \partial_x \phi = 0, \quad \partial_t \phi + a^2 \partial_x \rho = -\frac{\lambda}{2D}\frac{\phi|\phi|}{\rho}. \tag{3}$$

The gas dynamics on a pipeline segment are represented using (3), with a unique solution when any two of the boundary conditions $\rho(t,0) = \rho_0(t)$, $\phi(t,0) = \phi_0(t)$, $\rho(t,L) = \rho_L(t)$, or $\phi(t,L) = \phi_L(t)$ are specified. For both notational and numerical purposes, we first apply the dimensional transformations

$$\hat{t} = \frac{t}{\ell/a}, \quad \hat{x} = \frac{x}{\ell}, \quad \hat{p} = \frac{\rho}{\rho_0}, \quad \hat{\phi} = \frac{\phi}{a\rho_0}, \tag{4}$$

to yield a non-dimensional system

$$\partial_t \rho + \partial_x \phi = 0, \quad \partial_t \phi + \partial_x \rho = -\frac{\lambda\ell}{2D}\frac{\phi|\phi|}{\rho}, \tag{5}$$

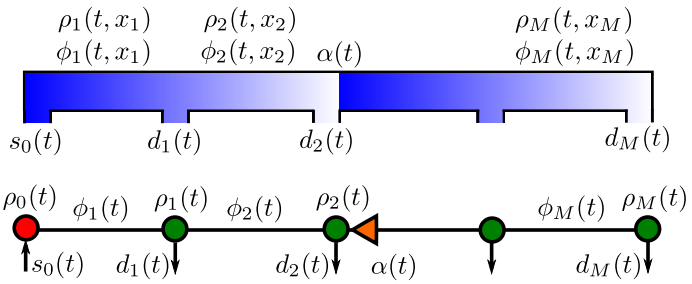


Figure 1. Illustration of a pipeline with injection $s_0$, a compressor $\alpha$, and withdrawals $d_i$. Top: The dynamical solution is determined by functions for pressure $\rho_i$ and mass flux $\phi_i$ on multiple domains, with boundary conditions associated with each withdrawal and compression. Shading illustrates density; Bottom: The continuous system is reduced to a graph representation with flows on links and densities at nodes.

in which the hats have been omitted for readability. In Sections 3-6 we use the non-dimensional units.

Because friction causes pressure to decrease along the pipeline, gas compressors are used to boost the pressure to maintain it above the minimum level required for delivery to customers. The compressors provide pipeline operators with the means to actuate the state of the transmission system. Because the size of a compressor station is very small compared to the distance of a pipeline, we model the action of a compressor as a multiplicative increase in density at a point $x = c$ with conservation of flow. This action is expressed as $\rho(t,c^+) = \alpha(t)\rho(t,c^-)$ and $\phi(t,c^+) = \phi(t,c^-)$, where $\alpha(t)$ is a time-dependent compression factor. We use the notation $h(c^-) = \lim_{x\nearrow c} h(x)$ and $h(c^+) = \lim_{x\searrow c} h(x)$. The compressor power is proportional to

$$C \propto \frac{1}{\eta}|\phi(t,c)|(\max\{\alpha(t),1\}^{2m} - 1) \tag{6}$$

with $0 < m < (\gamma-1)/\gamma < 1$ where $\gamma$ is the heat capacity ratio and $\eta$ is the compressor efficiency [11, 16]. Note that using this formulation, decompression ($\alpha(t) < 1$) does not require any power.

## 3 ECONOMIC TRANSIENT COMPRESSION

Consider a large-scale natural gas transmission pipeline with junctions distributed along its length at which the pressure can be boosted by a compressor or gas can be injected or withdrawn. Between such junctions the mass flux and density evolve according to (5). The sequence of segments connected at junctions can be considered as a graph $\mathcal{G} = (\mathcal{V}, \mathcal{E})$, where each segment is an edge $j \in \mathcal{E} = \{1,\dots,M\}$ that connects junctions $j-1, j \in \mathcal{V} = \{0,1,\dots,M\}$, as illustrated in Figure 1. We only consider chain graphs here, i.e., with $M = |\mathcal{E}|$ edges that connect $M+1 = |\mathcal{V}|$ nodes in a chain.

The state of the $j$th pipeline segment consists of density $\rho_j$ and flux $\phi_j$ defined on a time interval $\mathcal{T} = [0,T]$, and in the distance variable $x_j \in [0, L_j] = \mathcal{L}_j$. Defining the domain of the PDE solution for the $j$th pipe segment as $\mathcal{D}_j = \mathcal{T} \times \mathcal{L}_j$, the state functions are expressed as $\rho_j : \mathcal{D}_j \to \mathbb{R}^+$ and $\phi_j : \mathcal{D}_j \to \mathbb{R}$, which satisfy

$$\partial_t \rho_j + \partial_x \phi_j = 0, \qquad \forall\, j = 1,\dots,M, \tag{7}$$

$$\partial_t \phi_j + \partial_x \rho_j = -\frac{\lambda \ell}{2D}\frac{\phi_j|\phi_j|}{\rho_j}, \qquad \forall\, j = 1,\dots,M. \tag{8}$$

For simplicity, we assume that each junction $j = 0,1,\dots,M-1$ may have a compressor station that boosts the pressure of gas entering pipe segment $j+1 \in \mathcal{E}$ according to multiplicative compression ratios $\alpha_j : \mathcal{T} \to \mathbb{R}_+$ for $j = 0,\dots,M-1$. We denote by $s_0(t)$ the density of gas entering the supply terminal $0 \in \mathcal{V}$ before compression by $\alpha_0(t)$. Mass flux withdrawals (or injections, if negative) at remaining junctions $j \in \mathcal{V}_D = \mathcal{V} \setminus \{0\}$ are denoted by $d_j(t)$. The functions $\alpha_j(t)$, $d_j(t)$ and $s_0(t)$ create density and flux balance boundary conditions on (7)-(8) in the form of

$$\rho_{j+1}(t,0) = \alpha_j(t)\rho_j(t,L_j), \qquad j = 1,\dots,M-1 \tag{9}$$

$$\phi_{j+1}(t,0) = \phi_j(t,L_j) + d_j(t), \qquad j = 1,\dots,M-1 \tag{10}$$

$$\rho_1(t,0) = \alpha_0(t)s_0(t), \tag{11}$$

$$\phi_M(t,L_M) = d_M(t). \tag{12}$$

Our objective is to minimize compression costs $J_E$ of the form (6) over $\mathcal{T}$,

$$J_E = \sum_{j=1}^{M}\int_0^T \frac{1}{\eta}|\phi_j(t,0)|\big((\max\{\alpha_{j-1}(t),1\})^{2m} - 1\big)\mathrm{d}t. \tag{13}$$

We also impose constraints on the gas density and compression ratios,

$$\rho_j^{\min} \le \rho_j(t,x) \le \rho_j^{\max}, \qquad j = 1,\dots,M, \tag{14}$$

$$0 \le \alpha_j(t) \le \alpha_j^{\max}, \qquad j = 0,\dots,M-1. \tag{15}$$

In normal operations, we consider periodic boundary conditions in time, i.e.,

$$p_j(0,x_j) = p_j(T,x_j), \qquad j = 1,\dots,M, \tag{16}$$

$$\phi(0,x_j) = \phi(T,x_j), \qquad j = 1,\dots,M, \tag{17}$$

$$\alpha_j(0) = \alpha_j(T), \qquad j = 0,\dots,M-1, \tag{18}$$

which requires the gas withdrawals and injections to satisfy $d_j(0) = d_j(T)$ for $j = 1,\dots,M$, and $s_0(0) = s_0(T)$. For day-ahead operational planning, the time horizon of interest is on the order of $T = 24$ hours. The OCP takes the following formulation:

$$\begin{aligned} &\min_{\alpha_j,\,\forall j} J_E \text{ in (13)} \\ &s.t.\ \text{dynamic PDE constraints: (7)} - \text{(8)}, \\ &\quad \text{nodal boundary conditions: (9)} - \text{(12)}, \\ &\quad \text{density and compression constraints: (14)} - \text{(15)}, \\ &\quad \text{time-periodicity: (16)} - \text{(18)}. \end{aligned} \tag{19}$$

The OCP (19) is analytically intractable, and is computationally challenging even in the case of $M = 1$, i.e., a single pipeline segment [25]. In the next section, we extend a model reduction for

flows on gas networks [23] to derive a control system to replace the constraints (7)-(8) and (9)-(12) in the OCP (19). This yields a tractable problem, as described in Section 6.

## 4 MODEL REDUCTION OF GAS PIPELINE DYNAMICS

We design a control system using a tractable yet accurate model of the PDEs (7)-(8) on a cascade of pipeline segments with boundary conditions (9)-(12) resulting from compression and/or gas injection or withdrawal, as shown in Figure 1. A segment of (non-dimensional) length $L$ is modeled as a lumped element by integrating (7)-(8) with respect to $x$,

$$\int_0^L (\partial_t \rho_j + \partial_x \phi_j)\mathrm{d}x = 0, \tag{20}$$

$$\int_0^L (\partial_t \phi_j + a^2 \partial_x \rho_j)\mathrm{d}x = -\frac{\lambda \ell}{2D}\int_0^L \frac{\phi_j|\phi_j|}{\rho_j}\mathrm{d}x, \tag{21}$$

with the integrals of $\partial_t$, $\partial_x$, and nonlinear terms evaluated using the trapezoid rule, the fundamental theorem of calculus, and averaging variables, respectively:

$$\frac{L}{2}(\tfrac{\mathrm{d}}{\mathrm{d}t}\rho_j^0 + \tfrac{\mathrm{d}}{\mathrm{d}t}\rho_j^L) = \phi_0 - \phi_L, \tag{22}$$

$$\frac{L}{2}(\tfrac{\mathrm{d}}{\mathrm{d}t}\phi_j^0 + \tfrac{\mathrm{d}}{\mathrm{d}t}\phi_j^L) = \rho_0 - \rho_L - \frac{\lambda \ell}{4D}\cdot L\frac{(\phi_j^0+\phi_j^L)|\phi_j^0+\phi_j^L|}{\rho_j^0+\rho_j^L}. \tag{23}$$

Here, $\rho_j^0$, $\phi_j^0$ and $\rho_j^L$, $\phi_j^L$ denote density and flux at the start and end of the $j$th segment, respectively.

Defining input and output flows $\phi_j^0$ and $\phi_j^L$, and densities $\rho_j^0 > 0$ and $\rho_j^L > 0$, equations (22)-(23) for each edge with boundary conditions (9)-(11) yield a differential-algebraic equation (DAE) system where

$$0 = \rho_{j+1}^0 - \alpha_j \rho_j^L, \tag{24}$$

$$d_j = \phi_j^L - \phi_{j+1}^0, \tag{25}$$

$$\frac{\frac{\mathrm{d}}{\mathrm{d}t}\rho_j^L + \frac{\mathrm{d}}{\mathrm{d}t}\rho_j^0}{2} = -\frac{\phi_j^L - \phi_j^0}{L_j}, \tag{26}$$

$$\frac{\frac{\mathrm{d}}{\mathrm{d}t}\phi_j^L + \frac{\mathrm{d}}{\mathrm{d}t}\phi_j^0}{2} = -\frac{\rho_j^L - \rho_j^0}{L_j} - \frac{\lambda_j \ell}{4D_j}\left(\frac{(\phi_j^L+\phi_j^0)|\phi_j^L+\phi_j^0|}{\rho_j^L+\rho_j^0}\right) \tag{27}$$

for each for each $j = 1,\ldots,M$, and $\rho_0^0 = \alpha_0 s_0$. Here (24) represents continuity of pressure at junctions with jumps in the case of compression, (25) represents nodal flow balance, and (26)-(27) represent edge dynamics.

We employ graph-theoretic notation from Section 3 to express (24)-(27) in matrix-vector form. For the graph $\mathcal{G}$, we define the weighted incidence matrix

$$B_{ij} = \begin{cases} 1 & \text{edge } j \text{ enters node } i, \text{ i.e., } j = i \\ -\alpha_j & \text{edge } j \text{ leaves node } i, \text{ i.e., } j = i+1 \\ 0 & \text{else} \end{cases} \tag{28}$$

as well as the incidence matrix $A = \mathrm{sign}(B)$. In addition, let $A_s$ and $B_s$ denote the first rows of $A$ and $B$, and let $A_d$ and $B_d$ denote the remaining rows. Then let $A_L$ and $A_0$ denote the positive and negative parts of $A_d$, so that $A_d = A_L + A_0$. Also, define the diagonal matrices $\Lambda$ and $K$ by $\Lambda_{ii} = L_i$ and $K_{ii} = \ell\lambda_i/D_i$, where $L_i$, $\lambda_i$, and $D_i$ are the nondimensional length, friction coefficient, and diameter of the $i$th pipe segment. Finally, define a function $g : \mathbb{R}^M \times \mathbb{R}_+^M \to \mathbb{R}^M$ by $g_j(x,y) = x_j|x_j|/y_j$. Then letting $\rho = (\rho_1^L,\ldots,\rho_M^L)^T$, $\phi_0 = (\phi_1^0,\ldots,\phi_M^0)^T$, $\phi_L = (\phi_1^L,\ldots,\phi_M^L)^T$, and $d = (d_1,\ldots,d_M)^T$, equations (24)-(27) are written as

$$d = A_L\phi_L + A_0\phi_0, \tag{29}$$

$$|B_s^T|\tfrac{\mathrm{d}}{\mathrm{d}t}s_0 + |B_d^T|\tfrac{\mathrm{d}}{\mathrm{d}t}\rho = -4\Lambda^{-1}\tfrac{1}{2}(\phi_L - \phi_0), \tag{30}$$

$$\tfrac{1}{2}(\tfrac{\mathrm{d}}{\mathrm{d}t}\phi_L + \tfrac{\mathrm{d}}{\mathrm{d}t}\phi_0) = -\Lambda^{-1}(B_s^T s_0 + B_d^T\rho) - Kg(\tfrac{1}{2}(\phi_L+\phi_0), |B_s^T|s_0 + |B_d^T|\rho). \tag{31}$$

Note that $A_d = A_L + A_0$ and $|A_d| = A_L - A_0$, so by defining $\phi = \frac{1}{2}(\phi_L+\phi_0)$ and $\phi_- = \frac{1}{2}(\phi_L - \phi_0)$ we may replace (29) with $d = A_d\phi + |A_d|\phi_-$, the right hand side of (30) with $-4\Lambda^{-1}\phi_-$, and the left hand side of (31) with $\frac{\mathrm{d}}{\mathrm{d}t}\phi$. Then multiplying (30) by $|A_d|\Lambda$ results in $|A_d|\Lambda|B_s^T|\frac{\mathrm{d}}{\mathrm{d}t}s_0 + |A_d|\Lambda|B_d^T|\frac{\mathrm{d}}{\mathrm{d}t}\rho = -4|A_d|\phi_- = 4(A_d\phi - d)$. The DAE system (29)-(31) may then be written as an ODE system

$$\tfrac{\mathrm{d}}{\mathrm{d}t}\rho = (|A_d|\Lambda|B_d^T|)^{-1}[4(A_d\phi - d) - |A_d|\Lambda|B_s^T|\tfrac{\mathrm{d}}{\mathrm{d}t}s_0], \tag{32}$$

$$\tfrac{\mathrm{d}}{\mathrm{d}t}\phi = -\Lambda^{-1}(B_s^T s_0 + B_d^T\rho) - Kg(\phi, |B_s^T|s_0 + |B_d^T|\rho), \tag{33}$$

where the element $\phi_j$ of $\phi = (\phi_1,\ldots,\phi_M)^T$ approximates the mass flux on the $j$th pipe segment. Note that $A_d \in \mathbb{R}^{M\times M}$, $B_d \in \mathbb{R}^{M\times M}$, and $\Lambda$ are full rank, hence $|A_d|\Lambda|B_d^T|$ is invertible. Time-varying parameters are gas withdrawals $d \in \mathbb{R}^M$, input density $s_0 \in \mathbb{R}_+$, and compressions $\alpha_0,\ldots,\alpha_{M-1}$ contained in $B_d$, where $\alpha_j, \neq 1$ only if node $j \in \mathcal{V}$ has an active compressor.

*Consistency.* For a pipeline of (dimensional) length L with no compression or intermediate withdrawals and $M$ segments of uniform length L/M, resulting in nodes at $x_j \in \{0, L/M, \ldots, L\}$, it can be shown that $W = |A_d|\Lambda|B_d^T|$ is tridiagonal with $W_{j,j-1} = L/(M\ell)$, $W_{j,j} = 2L/(M\ell)$, and $W_{j,j+1} = L/(M\ell)$, and matrix $A_d$ satisfies $(A_d)_{j,j} = 1$, $(A_d)_{j,j+1} = -1$. If at time $t$ we have $\rho_j(t) = \rho(t,x_j)$ and $\phi_j(t) = \phi(t, x_j - \frac{1}{2}\ell)$, then (32)-(33) yield

$$\frac{1}{4}(\tfrac{\mathrm{d}}{\mathrm{d}t}\rho_{j-1} + 2\tfrac{\mathrm{d}}{\mathrm{d}t}\rho_j + \tfrac{\mathrm{d}}{\mathrm{d}t}\rho_{j+1}) = -\frac{L}{M\ell}(\phi_j - \phi_{j+1}), \tag{34}$$

$$\tfrac{\mathrm{d}}{\mathrm{d}t}\phi_j = -\frac{L}{M\ell}(\rho_j - \rho_{j-1}) - \frac{\lambda\ell}{2D}\frac{\phi_j|\phi_j|}{\frac{1}{2}(\rho_j+\rho_{j-1})}, \tag{35}$$

as well as in $\rho_0 = s_0$ and $\phi_M = d_M$ at the boundaries. Taking the limit as $M \to \infty$ yields (7)-(8). It follows that the equations (32)-(33) are a consistent space-discretization of the PDEs (7)-(8) when $\alpha_j \equiv 1$ for $j = 0,\ldots,M-1$ and $d_j \equiv 0$ for all $j = 1,\ldots,M-1$. Thus the solution to (32)-(33) using an implicit Euler ODE integrator with a sufficiently small time-step will converge to the solution to (7)-(8) as $M$ is increased [26].

Equations (32)-(33) were used to simulate a basic pipeline model [7], with slow transients in input pressure and output flux

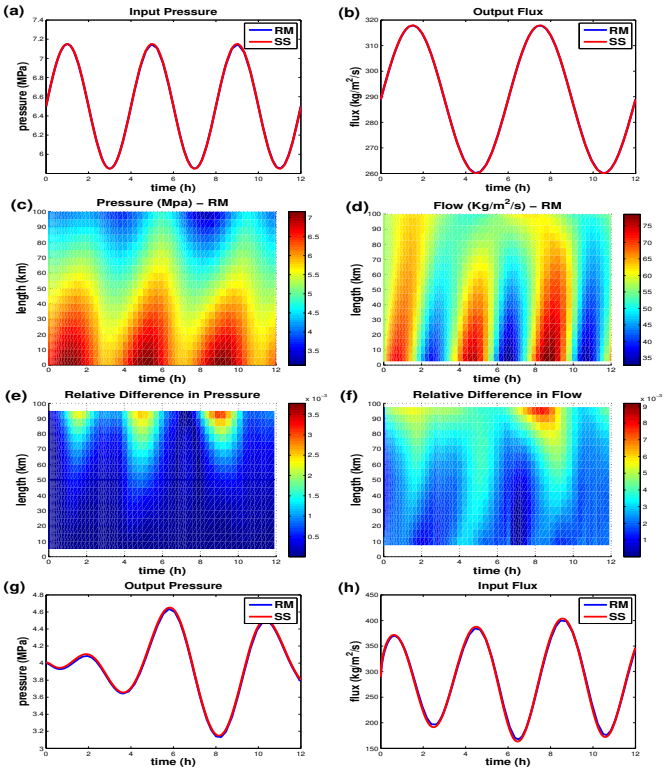


Figure 2. Simulation of pipeline with $L = 100$ km, $D = 0.5$ m, $a = 378$ m/s, $\lambda = 0.011$ and boundary conditions $s(t) = 4.5(1 + 0.1\sin(6\pi t/T))$ MPa and $d(t) = 289(1 + 0.1\sin(4\pi t/T))$ kg/m$^2$/s for $T = 12$ hours. Steady-state initial conditions are imposed. (a) input pressure $s(t)$ and (b) output flux $d(t)$; Computed (c) pressure and (d) flow solutions for reduced model with $M = 21$ space points and 85 time points using adaptive solver `ode15s` in MATLAB with relative error tolerance of $10^{-4}$; Relative difference in (e) pressure and (f) flow between the reduced model and split-step solution using 201 space points and 654 time points; (g) output pressure and (h) input flux solutions of the reduced model (RM) and split-step (SS) solutions differ by under 0.5%.

over 12 hours. The computation can be executed using the adaptive solver `ode15s` in MATLAB with error tolerance $10^{-4}$ on a 2.5 GHz core i5 processor in under 0.5 seconds. For boundary conditions in Figures 2a and 2b, the pressure and flow along the pipeline are shown in Figures 2c and 2d. In the next section, the reduced model (32)-(33) is validated by comparing this simulation to one using a split-step method for approximating solutions to this hyperbolic PDE system.

## 5 VALIDATION OF THE REDUCED DYNAMICAL MODEL USING A SPLIT-STEP METHOD

To validate the reduced ODE model (32)-(33), the simulation in Figure 2 is compared to a solution of the same system using a split-step integrator [27]. The operator splitting method [28] is used to produce an accurate numerical solution of the system (7)-(8) by splitting the operator corresponding to the PDE system into two simpler operators that can be applied exactly.

*Linear step.* The first operator corresponds to the solution of the homogeneous part of (7)-(8):

$$\partial_t \rho + \partial_x \phi = 0, \quad \partial_t \phi + \partial_x \rho = 0 \tag{36}$$

This is a linear hyperbolic system with unit propagation constant, which in dimensional form is the speed of sound $a$. This system can be solved exactly using the method of characteristics after the following diagonalization:

$$\vec{w} = \begin{pmatrix} q \\ \psi \end{pmatrix} = S \begin{pmatrix} \rho \\ \phi \end{pmatrix} \quad \text{where} \quad S = \frac{1}{\sqrt{2}} \begin{pmatrix} 1 & 1 \\ 1 & -1 \end{pmatrix}. \tag{37}$$

The decoupled equations are given by

$$\vec{w}_t + \begin{pmatrix} 1 & 0 \\ 0 & -1 \end{pmatrix} \vec{w}_x = 0 \text{ or } \begin{cases} q_t + q_x = 0, \\ \psi_t - \psi_x = 0, \end{cases} \tag{38}$$

with solutions propagating along characteristics $q(x,t) = q(x-t)$ and $\psi(x,t) = \psi(x+t)$. This yields

$$\rho(x,t) = \frac{q(x-t) + \psi(x+t)}{\sqrt{2}}, \tag{39}$$

$$\phi(x,t) = \frac{q(x-t) - \psi(x+t)}{\sqrt{2}}. \tag{40}$$

*Nonlinear step.* This operator propagates the ODE system

$$\partial_t \rho = 0, \quad \partial_t \phi = -\frac{\lambda \ell}{2D} \frac{\phi|\phi|}{\rho}, \tag{41}$$

which results in $\rho(t) = \rho_0$ and

$$\phi(t) = \frac{\phi(0)}{1 + t\frac{\lambda \ell}{2D}\frac{|\phi(0)|}{\rho_0}}. \tag{42}$$

*Split-Step Scheme.* We denote the action of the linear hyperbolic operator by $\hat{L}$ and the nonlinear operator by $\hat{N}$, and construct the numerical approximation of the solution by superimposing $\hat{L}$ and $\hat{N}$. This produces the system

$$\partial_t \mathbf{y} = (\hat{L} + \hat{N})\mathbf{y}, \tag{43}$$

where $\mathbf{y} = (\rho, \phi)^T$, which is solved exactly over a time step $h$ by

$$\mathbf{y}(t+h) = e^{(\hat{L}+\hat{N})h}\mathbf{y}(t). \tag{44}$$

Equation (44) is then approximated by

$$\mathbf{y}(t+h) = e^{(\hat{L}+\hat{N})h}\mathbf{y}(t) = e^{h\hat{L}}e^{h\hat{N}}\mathbf{y}(t) + O(h^2), \tag{45}$$

which has first order global truncation error. The second order split-step method amounts to symmetrization of (45) by

$$\mathbf{y}(t+h) = e^{\frac{h}{2}\hat{N}}e^{h\hat{L}}e^{\frac{h}{2}\hat{N}}\mathbf{y}(t) + O(h^3), \tag{46}$$

which gives second order global truncation error due to non-commutativity of the operators $\hat{L}$ and $\hat{N}$.

Solving the hyperbolic system (36) exactly provides a

significant advantage over traditional numerical discretization schemes, such as Crank-Nicholson, because no discretization error is introduced. Moreover, our numerical method and the physical model share the same dispersion relation $\omega = ak$, where $\omega$ is wave frequency, and $k = 2\pi/\lambda$ is the wave number for wavelength $\lambda$. Because of this property, the split-step scheme remains accurate even in situations with very rapid transients.

The simulation results obtained using the reduced model (32)-(33) shown in Figures 2c-2d are compared to solution using the above split-step method, and the difference is shown in Figure 2e-2f. Globally, the differences are less than 1%. In particular, the solutions at the pipe inlet and outlet are compared in Figure 2g-h, and differ by under 0.5%.

## 6 IMPLEMENTATION OF CONTROL METHOD

Equipped with the reduced model formulated in Section 4, we now reduce the ETC OCP (19) to a tractable form. The new dynamic constraints (32)-(33) replace the PDE constraints (7)-(8) and (9)-(12). The objective and remaining constraints are rewritten using the reduced model variables. Thus (13) becomes

$$J_E = \sum_{j=1}^{M} \int_0^T \frac{1}{\eta} |\phi_j(t)| \big( (\max\{\alpha_{j-1}(t), 1\})^{2m} - 1 \big) \mathrm{d}t, \qquad (47)$$

the density box constraints (14) become

$$\rho_j^{\min} \le \rho_j(t) \le \rho_j^{\max}, \qquad j = 1, \ldots, M, \qquad (48)$$

and the time-periodicity constraints are simplified to

$$p_j(0) = p_j(T), \qquad j = 1, \ldots, M, \qquad (49)$$
$$\phi(0) = \phi(T), \qquad j = 1, \ldots, M. \qquad (50)$$

Therefore the OCP (19) can be simplified to

$$\begin{aligned} \min_{\alpha_j, \forall j} \; & J_E \text{ in (47)} \\ s.t. \; & \text{reduced model constraints: (32)} - \text{(33)}, \\ & \text{density and compression constraints: (48) \& (15)}, \\ & \text{time-periodicity: (49)} - \text{(50) \& (18)}. \end{aligned} \qquad (51)$$

In this formulation, the system states are nodal densities $\rho = (\rho_1, \ldots, \rho_M)^T \in \mathbb{R}_+^M$ and edge fluxes $\phi = (\phi_1, \ldots, \phi_M)^T \in \mathbb{R}^M$, and the decision variable is the vector-valued function $\alpha = (\alpha_0, \ldots, \alpha_{M-1})^T$, where $\alpha_j(t) \equiv 1$ at all junctions without compression. The non-zero control functions are embedded in the time-varying coefficient matrices $B_s$ and $B_d$. While still a complex and analytically intractable optimization problem over a function space, the instantaneous state variables of the dynamic constraints in (51) are now finite vectors, rather than functions on continuous domains. The decision variables remain continuous functions, which still presents the challenge of approximating a continuous object using a finite computational representation.

Among numerous techniques used to discretize OCPs, pseudospectral (PS) methods stand out as particularly effective and versatile options [29]. In the context of optimal control, such techniques employ polynomial approximation to discretize a continuous-time OCP into a finite-dimensional constrained NLP [30]. Such methods have been widely applied to diverse problems in science and engineering [31]. The representation of continuous dynamics by polynomials provides spectral accuracy, and moreover, provides a strong guarantee of convergence. Specifically, given a sequence of optimal solutions to successively finely approximating NLPs, the corresponding sequence of interpolating polynomials converges to an optimal solution of the continuous OCP [24]. The PS approximation technique for optimal control problems is restated in Appendix A. The reduced formulation (51) can be approximated using the LGL PS method to yield a NLP. Here, $N+1$ time collocation points are used to represent each of the $M$ state functions $\phi_j$ and $\rho_j$, as well as $C \le M$ non-unit compressor variables $\alpha_j$, yielding a total of $(2M+C) \times (N+1)$ decision variables in the resulting nonlinear program. We omit the direct formulation of the NLP for (51), because the discretization is explained in Appendix A.

In the resulting NLP, the decision variables are the PS coefficients of the states and controls of the OCP, which in this case we express as $\bar{\rho} = (\bar{\rho}_1, \ldots, \bar{\rho}_M)^T \in \mathbb{R}_+^{M \times (N+1)}$, $\bar{\phi} = (\bar{\phi}_1, \ldots, \bar{\phi}_M)^T \in \mathbb{R}^{M \times (N+1)}$, and $\bar{\alpha} = (\bar{\alpha}_0, \ldots, \bar{\alpha}_{M-1})^T \in \mathbb{R}^{C \times (N+1)}$. For example, $\bar{\alpha}_j = (\bar{\alpha}_{j0}, \ldots, \bar{\alpha}_{jN})^T$ is the vector of Lagrange polynomial coefficients of the spectral approximation of the $j$th compression function, and $\alpha(t_k) = \bar{\alpha}_k = (\bar{\alpha}_{0k}, \ldots, \bar{\alpha}_{(M-1),k})^T$ is the vector of Lagrange coefficients for all compressors at a collocation time $t_k$. We then formulate the objective function and constraints in terms of the optimization variables. To expedite solution time, we also formulate the gradient of the objective and the Jacobian of the constraints to be provided to the solver. These four main functions are implemented in MATLAB, and then optimized using the interior point solver IPOPT version 3.11.8 running with the linear solver ma57 [32], called from a MATLAB interface. IPOPT is chosen because of its ability to leverage sparse linear algebra. The Jacobian of the constraints is sparse for the example in Section 7, with fewer than 1% non-zero entries. An error tolerance of $10^{-4}$ yields consistent results. Computation is done using a 3.33 GHz Intel i5 processor with 4 cores and 4GB RAM.

In order to guarantee a smooth, physically relevant solution, we penalize the square of the $L_2$ norms of the derivatives of the compression ratios by adding to the objective a term

$$J_S(\alpha) = \mu \sum_{j=0}^{M-1} ||\tfrac{\mathrm{d}}{\mathrm{d}t}\alpha_j||_2^2 = \mu \sum_{j=0}^{M-1} \int_0^T (\tfrac{\mathrm{d}}{\mathrm{d}t}\alpha_j(t))^2 \mathrm{d}t \qquad (52)$$

$$\approx \mu \frac{2}{T} \sum_{j=0}^{M-1} \sum_{i=0}^{N} \left( \sum_{k=0}^{N} D_{ik} \bar{\alpha}_{jk} \right)^2 w_i, \qquad (53)$$

where $\bar{\alpha}_j = (\bar{\alpha}_{j0}, \ldots, \bar{\alpha}_{jN})^T$ are the coefficients of the $j$th compression function, and $\mu$ is a relative weighting coefficient. The cost term $J_S$ is eliminated when discussing objective values.

The following basic case study demonstrates our implementation, and supports the security and economic necessity of con-

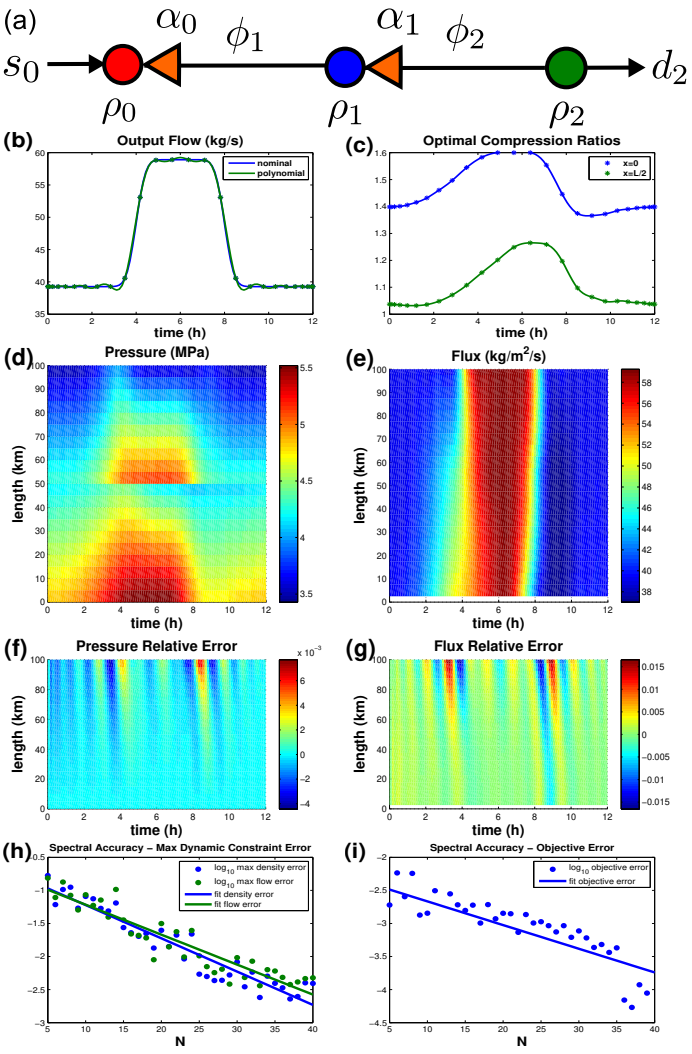


Figure 3. Optimization of a pipeline with $L = 100$ km, $D = 0.5$ m, $a = 378$ m/s, $\lambda = 0.011$, and pressure bounded in $[500, 800]$ psi. $s_0(t) = 500$ psi. (a) compressors at $x = 0$ and $x = L/2$; (b) $d_2(t)$ ramps smoothly up 50% during 1 hour from 200 kg/m$^2$/s starting at $t = 3.5$ hours, then back down during 1 hour starting at 7.5 hours; (c) optimal compression obtained by solving the NLP (51) with $M = 20$ space points and $N = 25$ LGL collocation points in time; (d) pressure and (e) flux in the pipeline for the optimal solution; Relative difference in (f) pressure and (g) flux from the collocation solution and simulation with the reduced model (32)-(33) given the compression solution is under 1.5%. Spectral accuracy is seen in exponential drop of (h) maximum error in dynamic constraints and (i) objective function error.

sidering transient dynamics in gas pipeline optimization.

*Example 1.* As a preliminary test of the PS method for solving the OCP (51), consider a pipeline with the parameters in Figure 2, but now with controllable compressors at the inlet $x = 0$ and the midpoint $x = L/2$. Gas is supplied at $x = 0$ at a pressure of $s_0 \equiv 500$ psi, and withdrawn at $x = L$ with time-varying output flux shown in Figure 3b over a $T = 12$ hour cycle. For gas at temperature between 0 and 30°C, the average heat capacity ratio is $\gamma \approx 2.75$ [33], so we use $m = 0.6154$ and (for simplicity) $\eta = 1$ in (47). Pressure is bounded within $[500, 800]$ psi.

*Transient Optimization.* The parameters and results of the optimization and simulation are shown in Figure 3. For $M = 20$, $C = 2$, and using $N = 25$ time points, the problem involves 1092 variables, 4.5% nonzero Jacobian entries, and requires 18 seconds to solve with objective value of 67.113. The control solutions are validated by applying them to the reduced model (32)-(33), and comparing the pressure and flux solutions to the collocation solutions obtained from the optimization. The relative difference is less than 1.5%, as shown in Figures 3f-3g. In addition, the spectral accuracy of polynomial approximation is shown by plotting the base 10 log of maximum error in dynamic constraints and objective function error in Figures in 3h and Figures in 3i as a function of PS discretization order. The decay in error fits an exponential decay, as expected.

*Static Optimal Gas Flow (OGF).* By using a time discretization of $N = 1$, the NLP obtained using the PS scheme reduces to the static OGF problem [16]. Taking the mean of the withdrawal flux in Figure 3b yields 233.33 kg/m$^2$/s and solving the static OGF leads to compression ratios of 1.485 at $x = 0$ and 1.077 at $x = L/2$, with objective value of 60.261. However, simulating the system with these compression ratios and applying the actual flux function in Figure 3b results in a minimum density of 248.75 psi, which is far below the minimum bound of 500 MPa. Such dramatic drops of pressure below intended levels are in fact observed with current operational practices [34].

*Constant Compression with Dynamic Constraints.* Our method can also be used to obtain a constant compression solution that satisfies the pressure bounds given transient injections and withdrawals. This is done by modifying the ETC problem to have a constant decision variable for each compression ratio, while the state variables remain time-dependent functions. Applying this change to Example 1, we find no feasible solution for this problem when pressure is bounded below 800 psi, even if the lower bound is relaxed. If the upper bound is increased to 1000 psi, there are feasible compression ratios of 1.618 at $x = 0$ and 1.166 at $x = L/2$, with objective value of 84.89.

## 7 LARGE-SCALE PIPELINE OPTIMIZATION

To demonstrate the feasibility of our technique for optimal control of pipeline dynamics in a real-world setting, we consider a case study of gas transport over the main pipeline of the Williams-Transco system through zones 5 and 6, which is shown in blue in Figure 5b. This section of the pipeline transports gas from the border of Georgia and South Carolina to a terminal near New York City, and contains 90 junctions where gas is injected or withdrawn, as well as 26 compressor stations [35]. We begin with the data set used in a previous study of the static OGF on the same zones of the pipeline network [16]. The balanced steady-state nominal injections and withdrawals into the system, as well as compressor station locations, are shown in Figure 5a. Additional nodes are added to the model so that edge distance is below

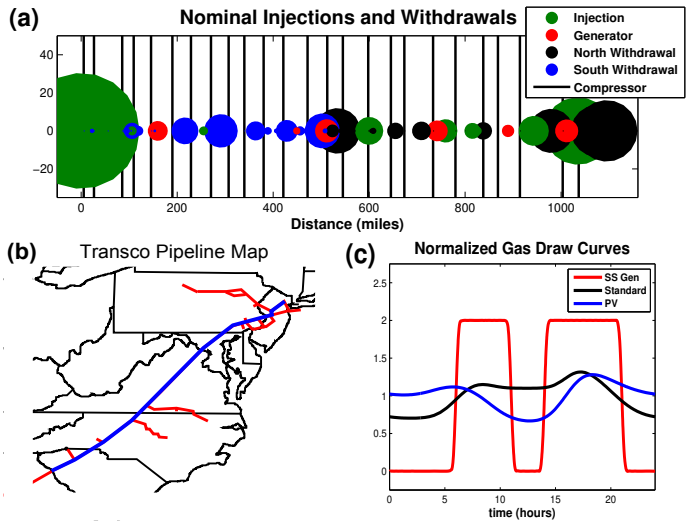


Figure 4. Optimization of Williams-Transco zones 5 and 6 main pipeline. (a) The area of circles illustrates magnitude of nominal mass flux injections (blue) and withdrawals (red), and lines denote compressors; (b) Geographical location of pipeline (blue) from North Carolina to New York; (c) Gas withdrawal curves: single cycle (SC) power plant (red), typical load curve (black), "duck curve" with high photovoltaic (PV) penetration (blue).

10 miles, so that the model appropriately resolves transients on the space-time scale of interest. We then suppose that injections are constant, while withdrawals are weighted according to three time-varying profiles representative of natural gas use shown in Figure 5c. These include the "duck curve", which is observed with large penetration of photovoltaic (PV) power sources, and a typical on/off profile of a single-cycle gas turbine. Crucially, the pressure throughout the line must be bounded between 500 and 800 psi, and compression ratio is confined to the interval $[1, 2]$.

*Transient Optimization.* The complete transient problem has $(2M+C)\times(N+1) = 8736$ variables, with 0.59% nonzero Jacobian entries, and requires 108 minutes to solve to adequate accuracy and smoothness. The optimal compressions are shown in Figure 5b, and the pressure and flux along the entire pipeline are given in Figure 5c and Figure 5d. The objective value is 1891.9, and all constraints are satisfied.

*Static Optimal Gas Flow.* As for Example 1, we can create the fully static case by assuming that all parameters are constant. This can be solved in 14 seconds with an objective value of 1765.7. Again, as before, applying the constant controls to the case with transient injections results in large violations of the pressure constraints, i.e., down to 273.9 psi and up to 946.3 psi.

*Constant Compression with Dynamic Constraints.* When we attempt to solve the transient problem using constant compression ratios, no feasible solution can be found unless the maximum pressure is relaxed to 1000 psi, in which case a solution is obtained in about 8 minutes, with objective value 1596.6.

The solutions corresponding to the (1) fully static, (2) constant compression with relaxed-pressure bound, and (3) transient cases are compared in Figure 5a, with bars denoting the variation

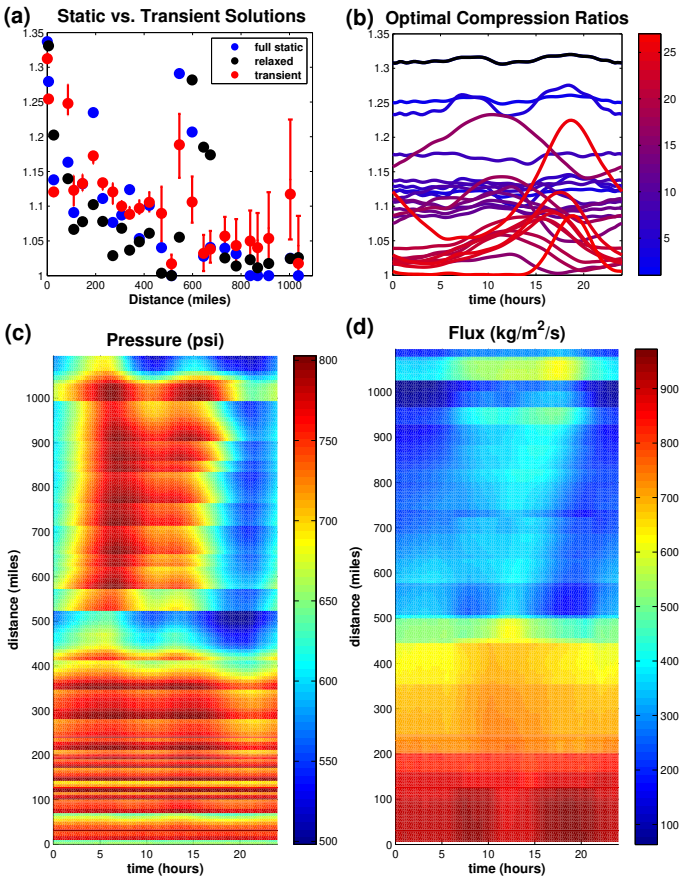


Figure 5. Optimization of Williams-Transco pipeline zones 5 and 6 main line. (a) Comparison of static approximation, static compression, and transient solutions; (b) Optimal pressure boost from 500 psi at input (black) and optimal compressor ratios from beginning (blue) to end (red); Optimal pressure (c) and Flux (d) along the pipeline when the transient solutions in (b) are applied.

of compressions in the transient case. These results are qualitatively similar to those observed for Example 1.

## 8 CONCLUSION

The control system model, simulation technique, and optimal control scheme described above have been demonstrated to be tractable, accurate, and efficient for modeling, analysis, and optimization of transient dynamics of compressible gas flow in a large-scale pipeline system. Based on the examples, we can conclude that optimization using steady-state assumptions, although useful for long-range planning, will result in drastically infeasible solutions for the actual short-term transient regime. Moreover, seeking a static solution while properly accounting for transient dynamics is infeasible for realistic pressure constraints. This creates a strong case for implementing transient compression solutions in operational planning for gas pipeline systems. In the current form, our approach already yields a significant qualitative and quantitative improvement over previously

published methods, as well as current industry standards. Specifically, a significant increase in effective pipeline capacity and operational security can be achieved given the highly variable consumptions currently observed in the gas transmission system. Further developments involve extension of the methodology to optimize flows over complex pipeline networks [36], to provide robust performance guarantees under uncertainty, and account for system-wide stochastic effects. The path forward requires obtaining the theoretical guarantees and computational efficiency such as those available for the static case [16], as well as formulating problems related explicitly to throughput.

## A PSEUDOSPECTRAL OPTIMAL CONTROL

Consider an optimal control problem (OCP) defined by

$$\min_u \; J(x,u) = \int_0^T \mathcal{L}(t,x(t),u(t))dt, \tag{54}$$

$$\text{s.t. } \dot{x}(t) = f(t,x(t),u(t)), \tag{55}$$

$$e(x(0),x(T)) = 0, \tag{56}$$

$$g(x(t),u(t)) \leq 0, \tag{57}$$

on the time interval $\mathcal{T} = [0,T]$. The running cost $\mathcal{L} \in C^\kappa$ is in the space $C^\kappa$ of continuous functions with $\kappa$ classical derivatives, and the dynamic constraints $f \in C_n^{\kappa-1}$ are in the space $C_n^{\kappa-1}$ of $n$-vector valued $C^{\kappa-1}$ functions, with respect to the state, $x(t) \in \mathbb{R}^n$, and control, $u(t) \in \mathbb{R}^m$. The functions $e$ and $g$ are terminal and path constraints, respectively. The admissible set for controls $u$ includes the piecewise $C_m^\kappa$ functions on $\mathcal{T}$. For mathematical details, refer to [24]. We now derive a direct collocation procedure for constructing a finite-dimensional nonlinear program (NLP) that approximates (54)-(57).

Direct collocation methods use polynomial interpolation to approximate continuous functions based on values at a set of collocation points $t_k$. We use Lagrange polynomials to approximate the states $x$ and controls $u$,

$$x(t) \approx \widehat{x}_N(t) = \textstyle\sum_{k=0}^N \bar{x}_k \ell_k(t), \tag{58}$$

$$u(t) \approx \widehat{u}_N(t) = \textstyle\sum_{k=0}^N \bar{u}_k \ell_k(t). \tag{59}$$

Lagrange interpolation polynomials satisfy $\ell_k(t_i) = \delta_{ki}$, where $\delta_{ki}$ is the Kronecker delta function [29]. It follows that $x(t_k) = \widehat{x}_N(t_k) = \bar{x}_k$ and $u(t_k) = \widehat{u}_N(t_k) = \bar{u}_k$, so the physical meaning of the interpolating polynomial coefficients $\bar{x}_k$ and $\bar{u}_k$ are the values of the state and control variables at the collocation points.

In addition to providing a finite-dimensional approximation of the problem (54)-(57), the Lagrange polynomial collocation scheme must be designed so that the integral in (54) and the derivative in (55) are computed accurately. The former can be approximated using Legendre-Gauss quadrature, leading to the choice of Legendre polynomials as the orthogonal basis for the PS method. Furthermore, the Legendre-Gauss-Lobatto (LGL) quadrature points are chosen, because the endpoints of the interval are included. This permits the terminal constraints to be specified within the discretization scheme. The LGL quadrature rule for a function $f : [-1,1] \to \mathbb{R}$ is given by

$$\int_{-1}^1 f(t)dt \approx \sum_{i=1}^N f(t_i)w_i, \qquad w_i = \int_{-1}^1 \ell_i(t)dt, \tag{60}$$

and is exact if the integrand $f \in \mathbb{P}_{2N-1}$ and the nodes $t_i \in \Gamma^{LGL}$, where $\mathbb{P}_{2N-1}$ denotes the set of polynomials of degree at most $2N-1$ and where $\Gamma^{LGL} = \{t_i : \dot{L}_N(t)|_{t_i} = 0, i = 1,\ldots N-1\} \bigcup \{-1,1\}$ are the $N+1$ LGL nodes determined by the derivative of the $N^{\text{th}}$ order Legendre polynomial, $\dot{L}_N(t)$, and the interval endpoints [29]. Note that the OCP requires evaluation of the running cost and satisfaction of dynamic constraints over the interval $\mathcal{T} = [0,T]$, whereas Legendre polynomials form a basis on the domain $[-1,1]$. In order to apply the LGL PS scheme, time is re-scaled by $\tilde{t} = (2t-T)/T$.

The Lagrange interpolating polynomials on the LGL collocation nodes can be re-written in terms of the Legendre polynomial basis, in order to endow the scheme with derivative and spectral accuracy properties of orthogonal polynomials. Given $t_k \in \Gamma^{LGL}$, we can express the Lagrange polynomials as [37]

$$\ell_k(t) = \frac{1}{N(N+1)L_N(t_k)} \frac{(t^2-1)\dot{L}_N(t)}{t-t_k}.$$

The derivative of (58) at $t_j \in \Gamma^{LGL}$ is then

$$\frac{d}{dt}\widehat{x}_N(t_j) = \sum_{k=0}^N \bar{x}_k \dot{\ell}_k(t_j) = \sum_{k=0}^N D_{jk}\bar{x}_k, \tag{61}$$

where $D$ is the constant differentiation matrix with elements $D_{ik} = \dot{\ell}_k(t_i)$. Using the equations (58), (59), (60), and (61), the OCP (54)-(57) is written as the following NLP, in which the decision variables are the polynomial interpolation coefficient vectors $\bar{x} = (\bar{x}_0,\ldots,\bar{x}_N)$ and $\bar{u} = (\bar{u}_0,\ldots,\bar{u}_N)$:

$$\min \; \bar{J}(\bar{x},\bar{u}) = \sum_{k=0}^N \frac{T}{2}\mathcal{L}(\bar{x}_k,\bar{u}_k)w_k \tag{62}$$

$$\text{s.t. } \sum_{k=0}^N D_{ik}\bar{x}_k = \frac{T}{2}f(t_i,\bar{x}_i,\bar{u}_i) \qquad \forall\, i = 0,1,\ldots,N \tag{63}$$

$$e(\bar{x}_0,\bar{x}_N) = 0 \tag{64}$$

$$g(\bar{x}_k,\bar{u}_k) \leq 0 \qquad \forall\, k = 0,1,\ldots,N \tag{65}$$


## ACKNOWLEDGEMENTS

The authors thank Alexander Korotkevich for ideas including the split-step method, and thank Russell Bent, Sidhant Misra, and Michael Fisher for guidance on modeling the Williams-Transco pipeline system. This work was carried out under the auspices of the National Nuclear Security Administration of the U.S. Department of Energy at Los Alamos National Laboratory under Contract #DE-AC52-06NA25396, and was partially supported by Defense Threat Reduction Agency Basic Research Project #10027-13399 and by the Advanced Grid Modeling Program in the U.S. Department of Energy Office of Electricity.

## REFERENCES


[1] MITEI, 2013. Growing concerns, possible solutions: The interdependency of natural gas and electricity systems.

[2] Chertkov, M., Fisher, M., Backhaus, S., Bent, R., and Misra, S., 2015. "Pressure fluctuations in natural gas networks caused by gas-electric coupling". In 48th Hawaii International Conf. on System Sciences (HICSS), IEEE.

[3] Wylie, E., and Streeter, V., 1978. *Fluid transients*. McGraw-Hill.

[4] Osiadacz, A., 1984. "Simulation of transient gas flows in networks". *International Journal for Numerical Methods in Fluids,* ***4***(1), pp. 13–24.

[5] Dorao, C., and Fernandino, M., 2011. "Simulation of transients in natural gas pipelines". *Journal of Natural Gas Science and Engineering,* ***3***(1), pp. 349–355.

[6] Thorley, A. R., and Tiley, C. H., 1987. "Unsteady and transient flow of compressible fluids in pipelinesa review of theoretical and some experimental studies". *International Journal of Heat and Fluid Flow,* ***8***(1), pp. 3–15.

[7] Herty, M., Mohring, J., and Sachers, V., 2010. "A new model for gas flow in pipe networks". *Mathematical Methods in the Applied Sciences,* ***33***(7), pp. 845–855.

[8] Seleznev, V. E., and Pryalov, S. N., 2014. "Computational fluid dynamics of trunklines systems". *M.: KRASAND*.

[9] Behbahani-Nejad, M., and Bagheri, A., 2010. "The accuracy and efficiency of a matlab-simulink library for transient flow simulation of gas pipelines and networks". *Journal of Petroleum Sci. and Eng.,* ***70***(3), pp. 256–265.

[10] Chapman, K., et al., 2005. *Virtual pipeline system testbed to optimize the US natural gas transmission pipeline system*. United States. Department of Energy.

[11] Wong, P., and Larson, R., 1968. "Optimization of natural-gas pipeline systems via dynamic programming". *Automatic Control, IEEE Transactions on,* ***13***(5), pp. 475–481.

[12] Rothfarb, B., et al., 1970. "Optimal design of offshore natural-gas pipeline systems". *Operations research,* ***18***(6), pp. 992–1020.

[13] Luongo, C., et al., 1991. "Optimizing the operation of gas transmission networks". In *Computers in Engineering*.

[14] Midthun, K. T., et al., 2009. "Modeling optimal economic dispatch and system effects in natural gas networks". *The Energy Journal*, pp. 155–180.

[15] Borraz-Sanchez, C., 2010. "Optimization methods for pipeline transportation of natural gas". PhD thesis, Bergen Univ. (Norway).

[16] Misra, S., et al., 2014. "Optimal compression in natural gas networks: a geometric programming approach". *IEEE Transactions on Control of Network Systems*, p. 1.

[17] Babonneau, F., Nesterov, Y., and Vial, J.-P., 2014. "Design and operations of gas transmission networks". *Operations Research,* ***60***(1), pp. 34–47.

[18] Rachford, H., and Carter, R., 2000. "Optimizing pipeline control in transient gas flow". *Pipeline Sim. Interest Group*.

[19] Ehrhardt, K., and Steinbach, M., 2005. *Nonlinear optimization in gas networks*. Springer.

[20] Steinbach, M., 2007. "On pde solution in transient optimization of gas networks". *Journal of computational and applied mathematics,* ***203***(2), pp. 345–361.

[21] Gopalakrishnan, A., and Biegler, L. T., 2013. "Economic nonlinear model predictive control for periodic optimal operation of gas pipeline networks". *Computers & Chemical Engineering,* ***52***, pp. 90–99.

[22] Devine, M. T., et al., 2014. "A rolling optimisation model of the uk natural gas market". *Networks and Spatial Economics,* ***14***(2), pp. 209–244.

[23] Grundel, S., et al., 2013. "Computing surrogates for gas network simulation using model order reduction". In *Surrogate-Based Modeling and Optimization*. Springer, pp. 189–212.

[24] Ruths, J., et al., 2011. "Convergence of a pseudospectral method for optimal control of complex dynamical systems". In 50th IEEE CDC, pp. 5553–5558.

[25] Herty, M., Kurganov, A., and Kurochkin, D., 2014. "Numerical method for optimal control problems governed by nonlinear hyperbolic systems of PDEs". *Comm. Math. Sci.*

[26] Verwer, J. G., and Sanz-Serna, J. M., 1984. "Convergence of method of lines approximations to partial differential equations". *Computing,* ***33***(3-4), pp. 297–313.

[27] Dyachenko, S., Korotkevich, A., et al. Numerical simulation of gas transportation networks using operator splitting method. In Preparation.

[28] Strang, G., 1968. "On the construction and comparison of difference schemes". *SIAM J. Numer. Anal.* ***5***, pp. 506–517.

[29] Canuto, C., et al., 2006. "Spectral methods". *Fundamentals in Single Domains, Springer*.

[30] Ross, I., and Fahroo, F., 2003. "Legendre pseudospectral approximations of optimal control problems". In *New Trends in Nonlinear Dynamics and Control and their Applications*. Springer, pp. 327–342.

[31] Ross, I. M., and Karpenko, M., 2012. "A review of pseudospectral optimal control: From theory to flight". *Annual Reviews in Control,* ***36***(2), pp. 182–197.

[32] Biegler, L. T., and Zavala, V. M., 2009. "Large-scale nonlinear programming using IPOPT". *Computers & Chem. Engineering,* ***33***(3), pp. 575–582.

[33] Campbell, J. M., Hubbard, R. A., and Maddox, R. N., 1988. *Gas conditioning and processing: the basic principles*. Campbell Petroleum Series.

[34] Tennessee GPC ISO NE presentation: 2011. http://isone.com/committees/comm_wkgrps/othr/egoc/mtrls/2011/mar302011/el_paso_isone_necpuc_032411.pdf.

[35] Williams-Transco Pipeline Informational Postings. http://www.1line.williams.com/Transco/index.html.

[36] Zlotnik, A., Chertkov, M., and Backhaus, S., 2015. "Optimal control of transient flow in natural gas networks". In 54th IEEE Conference on Decision and Control.

[37] Boyd, J. P., 2001. *Chebyshev and Fourier spectral methods*. Courier Corporation.